Science Advances

AAAS

advances.sciencemag.org/cgi/content/full/2/12/e1601838/DC1

Supplementary Materials for

General and programmable synthesis of hybrid liposome/metal nanoparticles

Jin-Ho Lee, Yonghee Shin, Wooju Lee, Keumrai Whang, Dongchoul Kim, Luke P. Lee, Jeong-Woo Choi, Taewook Kang

Published 16 December 2016, *Sci. Adv.* **2**, e1601838 (2016)
DOI: 10.1126/sciadv.1601838

This PDF file includes:

- fig. S15. Atomic percentages and absorbance spectra of liposome/Au-Ag hybrids and liposome/Au-Pd hybrids synthesized from different precursor molar ratios.
- fig. S16. Representative relative absorbance at the SPR peaks of LGNP, GNP, and GNR under a wide variety of biologically relevant solutions and representative relative absorbance of LGNP with time duration of up to 1 month.
- fig. S17. Viability of U-87 MG cells treated with LGNP and GNP solutions.
- fig. S18. Optical microscope images and Raman spectra obtained from various cells after being treated with LGNP and GNP.
- fig. S19. Fluorescent image and Raman spectra obtained from Alexa Fluor 546–stained U-87 MG cells, and optical microscope images and Raman maps obtained from Alexa Fluor 546–stained U-87MG cells after being treated with LGNP and GNP.
- table S1. Calculated relative atomic percentages of gold and oxygen atoms in LGNP.
- table S2. The number of metal atoms per unit volume in liposome/Au, liposome/Ag, and liposome/Pd hybrids, measured by inductively coupled plasma atomic emission spectroscopy.
- Reference (*51*)

Simulation details

We performed numerical simulations with commercial multiphysics software (COMSOL Multiphysics 4.4; COMSOL Inc.). The local concentrations of gold precursor and gold were calculated by diffusion equation with reaction as follows

$$\frac{\partial c_i}{\partial t} = \nabla \cdot (D_i \nabla c_i) + k_i c_1 {c_2}^{2/3} \quad (1)$$

where c_i, D_i, and, k_i are concentration, diffusivity, and rate constant of i^{th} species, respectively. Subscription index (i = 1, 2) correspond to the gold precursor and gold, respectively. The diameter of liposome and thickness of lipid bilayer were set to be 30 nm and 4.7 nm (*35*). Overall gold precursor concentration is 200 μM and the concentration of neutral gold precursor in the solution is 40 μM according to the equilibrium of hydrolysis progress (*37*) The diffusivity of neutral gold precursor (D_1) across the lipid bilayer was considered to be a function of depth inside the lipid bilayer based on the molecular dynamics simulation results (*38*, *39*) Since the diffusivity of neutral gold precursor across the lipid bilayer (1,2-distearoyl-sn-glycero-3-phosphocholine, DSPC) has not been reported, we calculate the diffusivity of neutral gold precursor by using the Stoke-Einstein relation for the diffusivity (*51*). Figure S7 shows the diffusivity of neutral gold precursor in lipid bilayer by using the diffusivity of acetamide in lipid bilayer (1,2-dipalmitoyl-sn-glycero-3-phosphocholine, DPPC). The molar mass of neutral gold precursor and acetamide are 321 and 59 g/mol, respectively. The influence of the difference in carbon chain length between DPPC (number of carbon: 16) and DSPC (number of carbon: 18) on the diffusivity of neutral gold precursor is considered as negligible. The diffusivity of gold (D_2) in the lipid bilayer is assumed to be zero because its charge prevents the gold from entering the hydrocarbon phase of the lipid bilayer. The rate constant, k_1 and k_2 are -10 and 10, respectively (*40*).

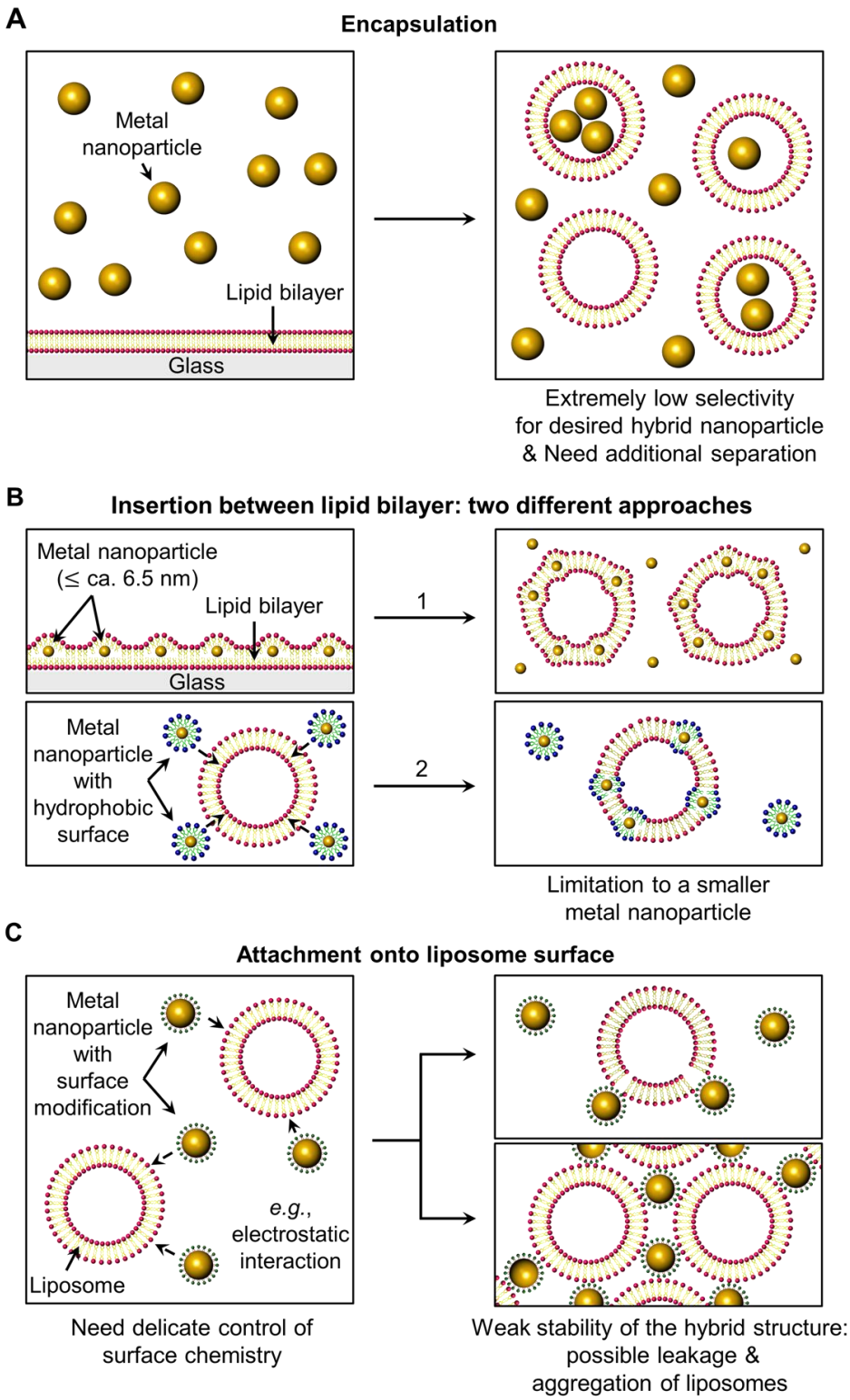

fig. S1. Schematic illustration of conventional approaches for liposome/metal hybrids and their critical limitations.

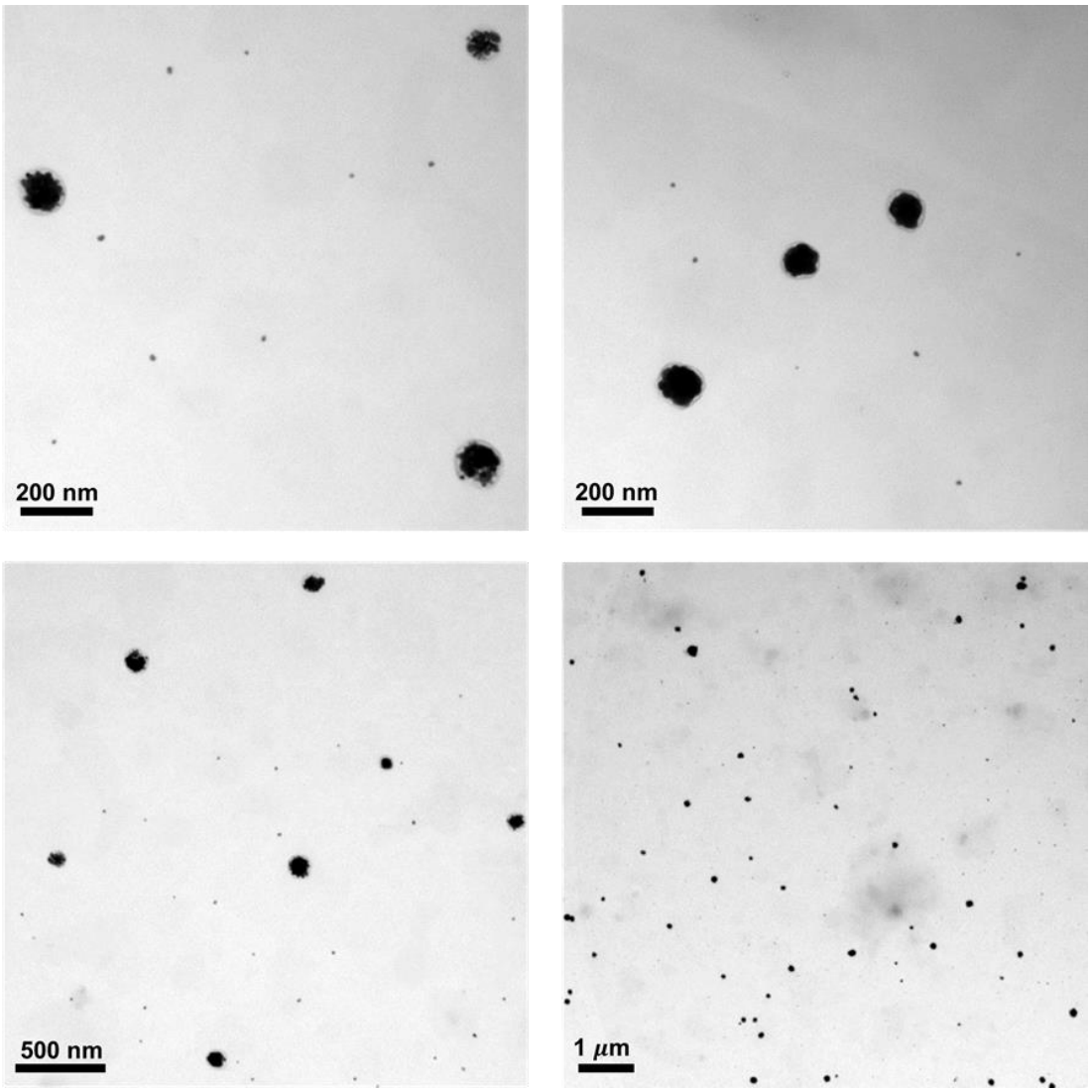

fig. S2. Additional TEM images of LGNP (using membrane filter with a pore diameter of 100 nm).

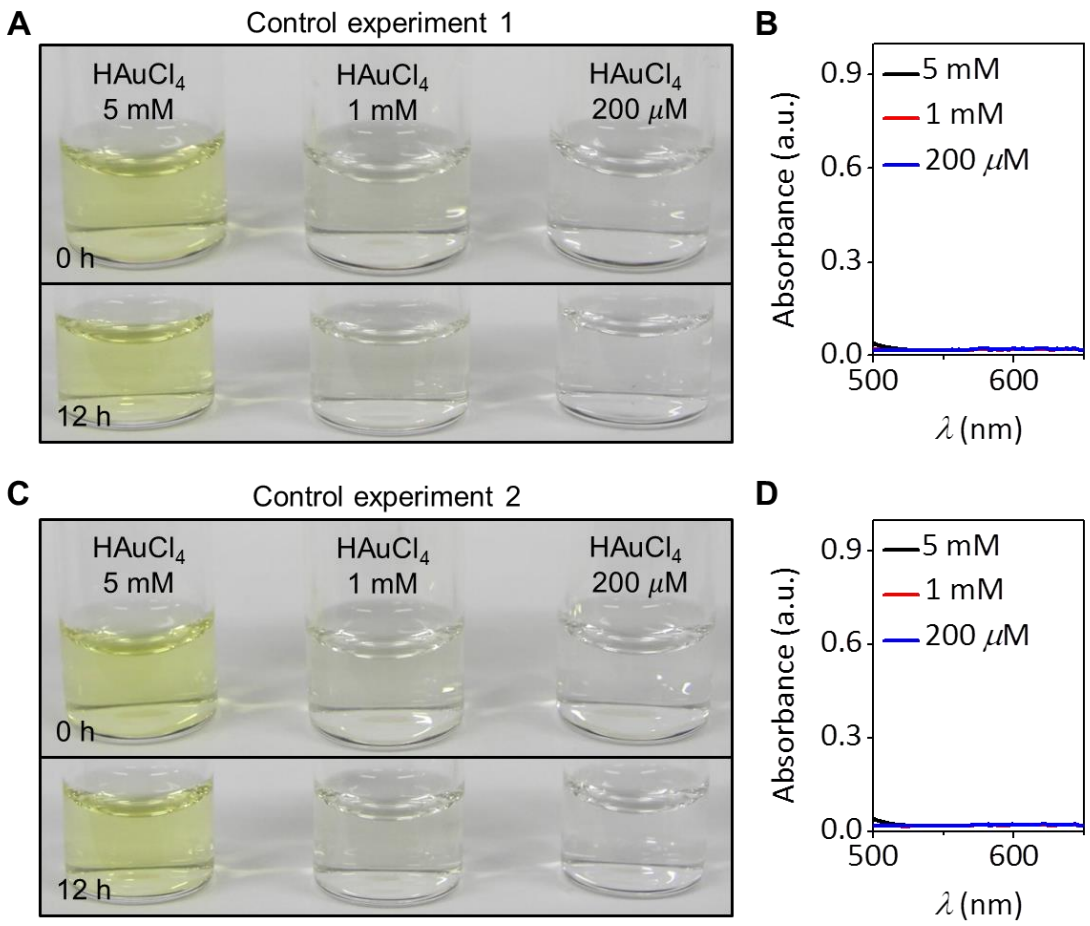

fig. S3. Photographs and absorbance spectra of control experiments. (A and **B)** Photographs (A) and UV-vis absorbance spectra (B) of mixed solutions of gold precursor and liposomes (without reducing agent). **(C** and **D)** Photographs (C) and absorbance spectra (D) of mixed solutions of gold precursor and reducing agent (trisodium citrate, 3 μM).

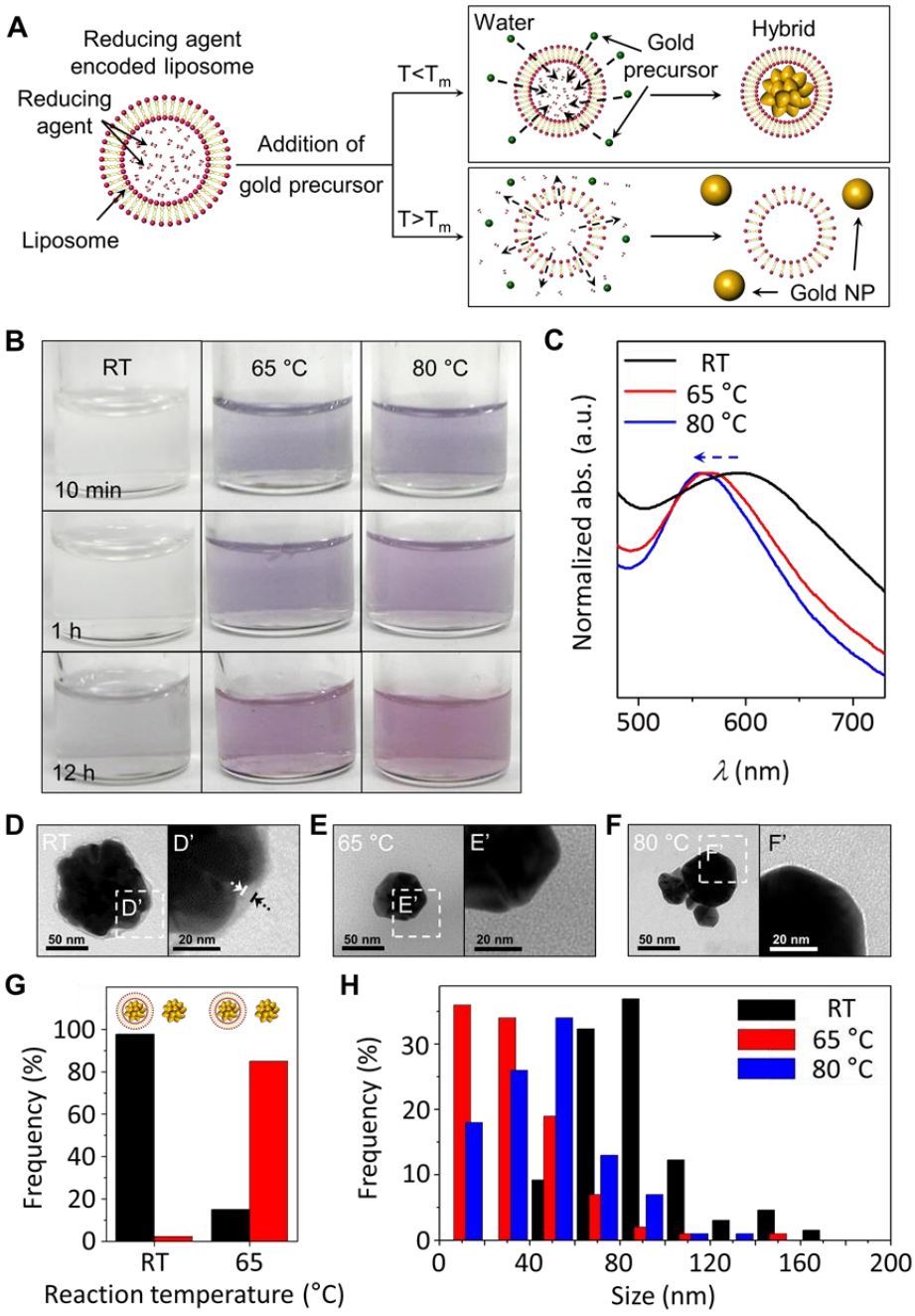

fig. S4. Reduction of gold ions above the transition temperature of lipid (DSPC). (A) Schematic illustration for comparison of the reduction of gold ions at room temperature (RT) and above transition temperature of the lipid (DSPC). **(B** and **C)** Representative photographs (B) and UV-vis absorbance spectra (C) of solutions of the nanoparticles synthesized at RT, 65 °C, and 80 °C. **(D**, **E**, and **F)** Representative TEM images of the

nanoparticles at RT (D), 65 °C (E), and 80 °C (F). **(G)** Frequency of nanoparticles with outer lipid layer at RT and 65 °C. **(H)** Size distributions at RT, 65 °C, and 80 °C.

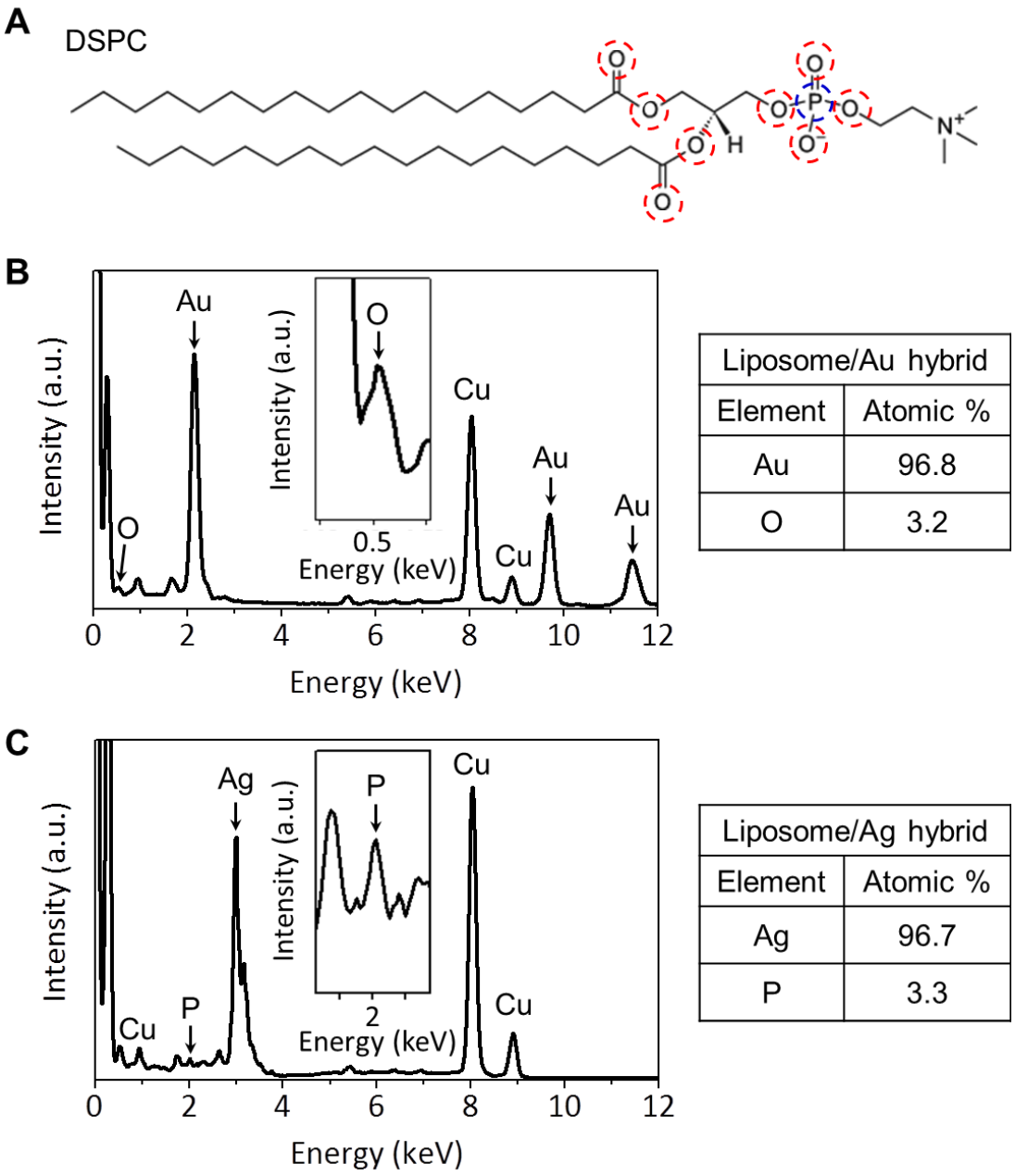

Liposome/Au hybrid	
Element	Atomic %
Au	96.8
O	3.2

Liposome/Ag hybrid	
Element	Atomic %
Ag	96.7
P	3.3

fig. S5. Molecular structure of DSPC and EDS spectrum and relative atomic percentages of as-prepared liposome/Au and liposome/Ag hybrid nanoparticles. (A) Molecular structure of 1,2-distearoyl-sn-glycero-3-phosphocholine (DSPC). **(B** and **C)** Energy-dispersive X-ray spectroscopy spectrum, and relative atomic percentages of as-prepared liposome/Au (B) and liposome/Ag (C) hybrid nanoparticles.

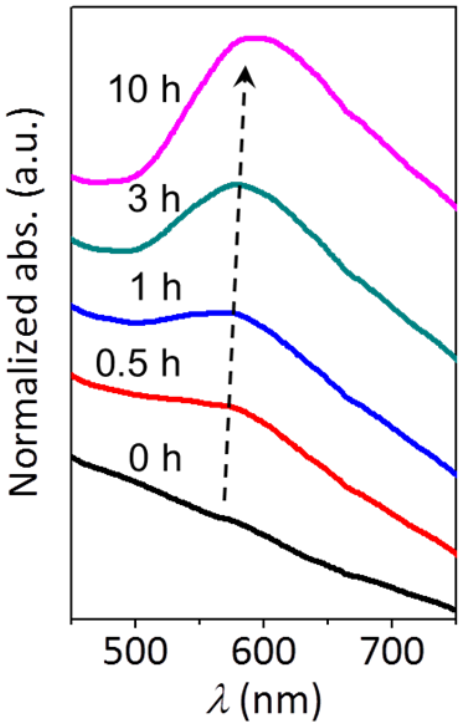

fig. S6. Time-dependent representative absorbance spectra of programmable liposome solution after the exposure with gold precursor.

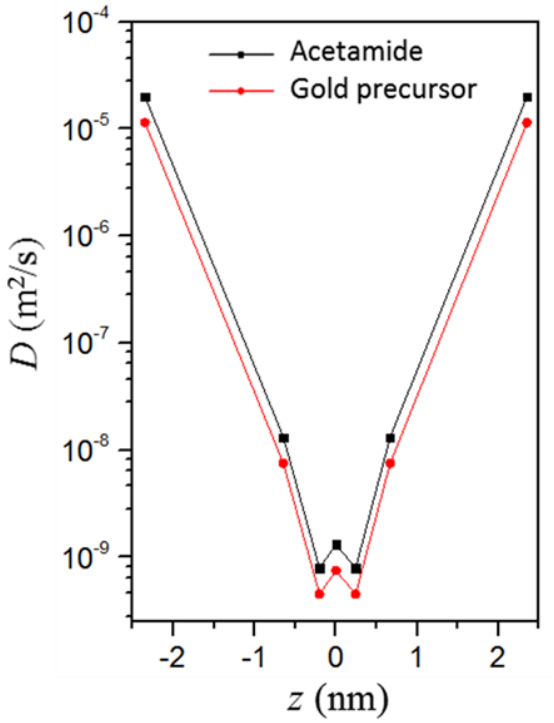

fig. S7. Diffusivities of acetamide and neutral gold ion complex. Diffusivities of acetamide and neutral gold ion complex that exist between lipid bilayers as a function of depth inside the lipid bilayer.

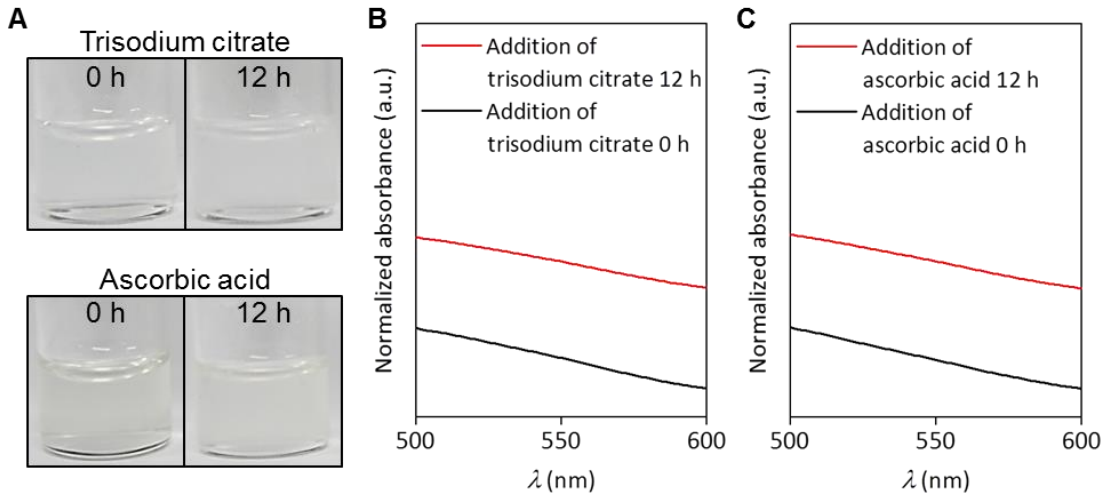

fig. S8. Photographs and absorbance spectra of solutions of the gold precursor–encoded liposome after addition of reducing agent. (A, **B**, and **C)** Photographs (A) and absorbance spectra (B and C) of solutions of the gold precursor-encoded liposome after addition of reducing agent (*i.e.*, trisodium citrate and ascorbic acid). The absorbance spectra were shifted along y-axis for clarity.

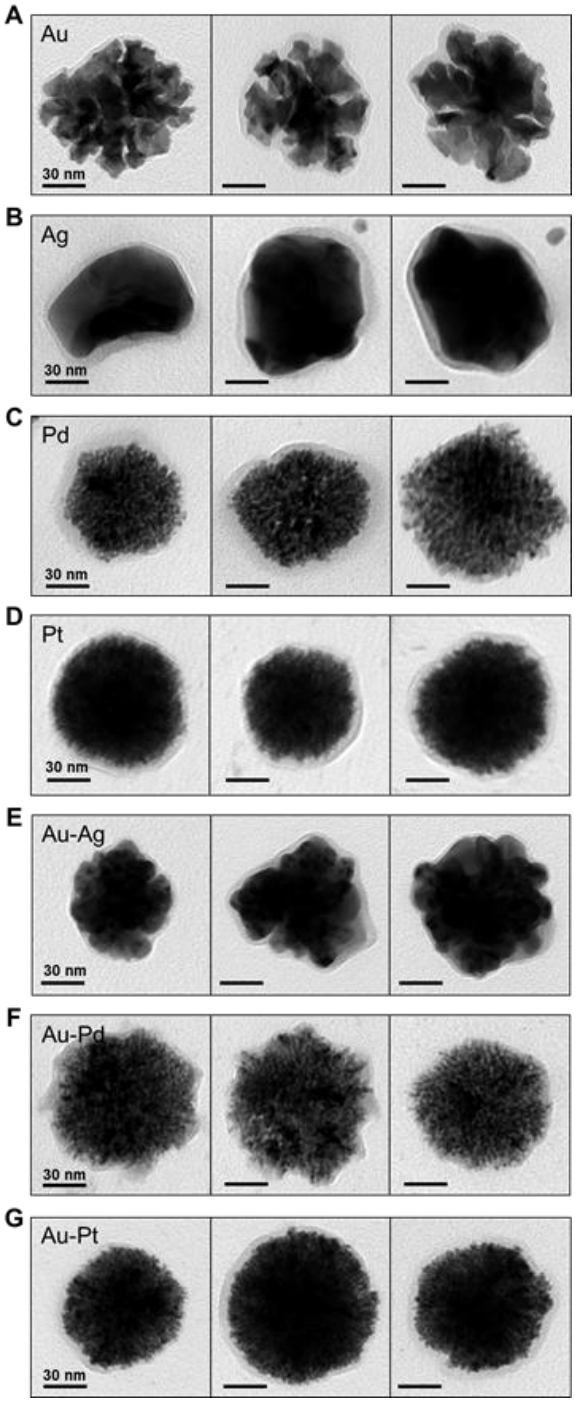

fig. S9. Additional TEM images of various liposome/metal hybrid nanoparticles.

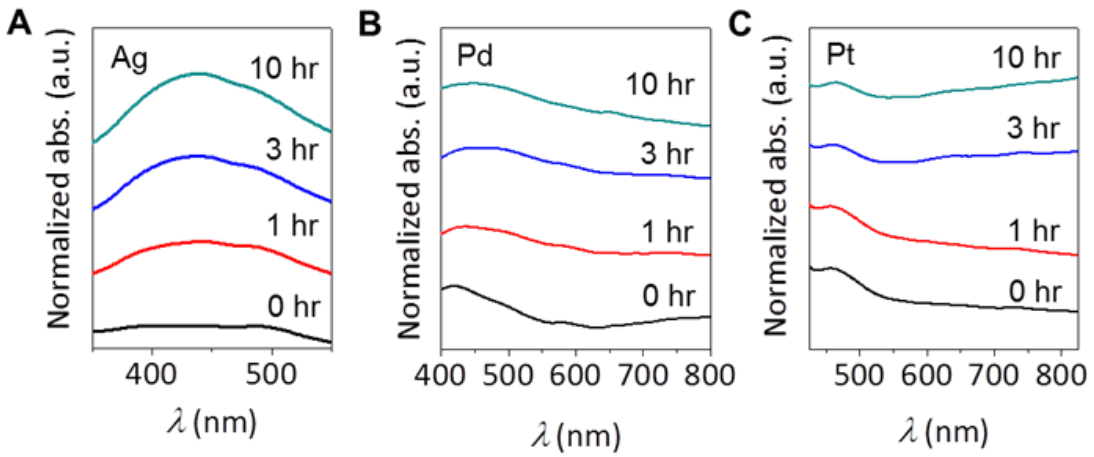

fig. S10. Representative time-resolved absorbance spectra of liposome/monometallic hybrid nanoparticle. (A, **B**, and **C)** Representative time-resolved absorbance spectra of liposome/Ag hybrid nanoparticle (A), liposome/Pd hybrid nanoparticle (B), liposome/Pt hybrid nanoparticle (C), respectively.

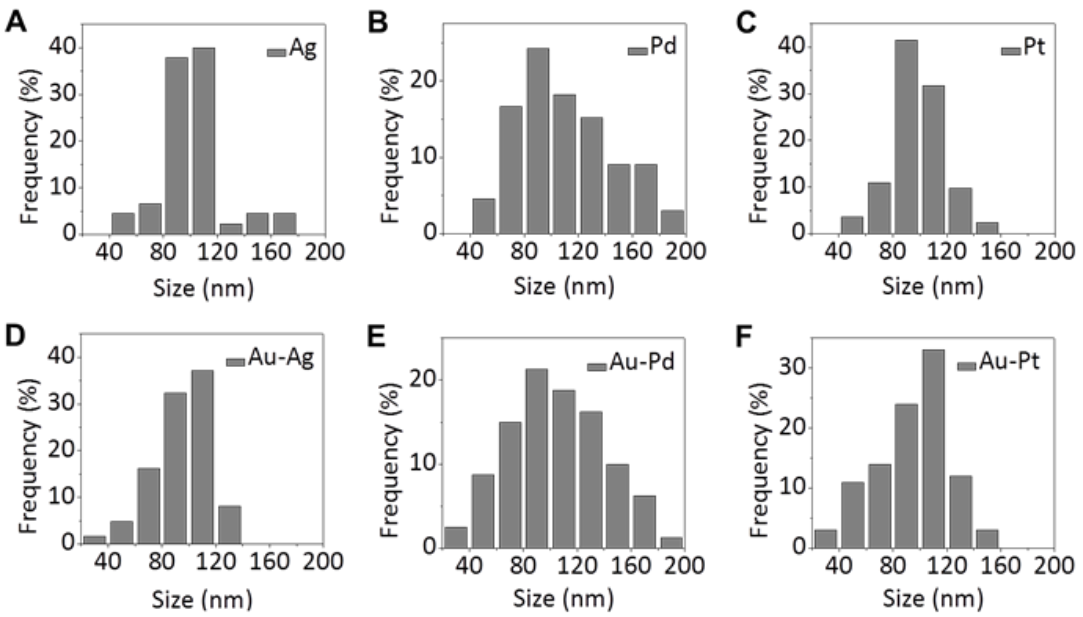

fig. S11. Size distributions of liposome/monometallic and liposome/bimetallic hybrids. (A, **B**, and **C)** Size distributions of liposome/monometallic hybrids (A: Ag, B: Pd, C: Pt). **(D**, **E**, and **F)** Size distributions of liposome/bimetallic hybrids (D: Au-Ag, E: Au-Pd, F: Au-Pt). For statistical analyses, 70 particles are randomly selected.

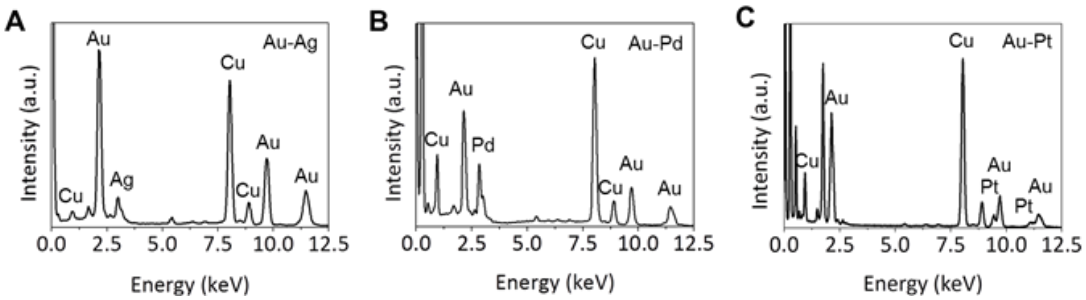

fig. S12. EDS spectra of liposome/bimetallic hybrids. (A, **B**, and **C)** EDS spectra of liposome/bimetallic hybrids (A: Au-Ag, B: Au-Pd, C: Au-Pt).

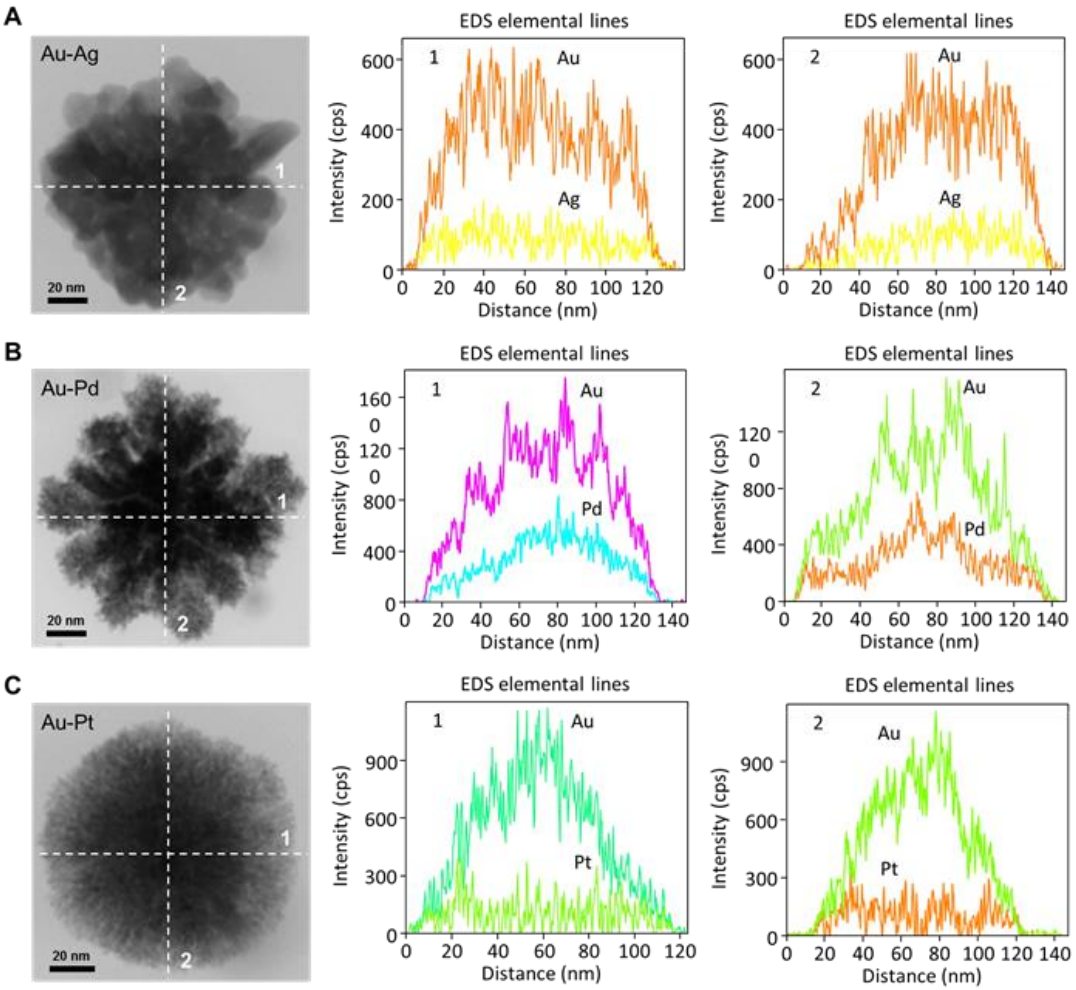

fig. S13. Representative TEM images and corresponding EDS elemental line profiles of liposome/bimetallic hybrids. (A, **B**, and **C)** Representative TEM images and corresponding EDS elemental line profiles of liposome/bimetallic hybrids (A: Au-Ag, B: Au-Pd, C: Au-Pt).

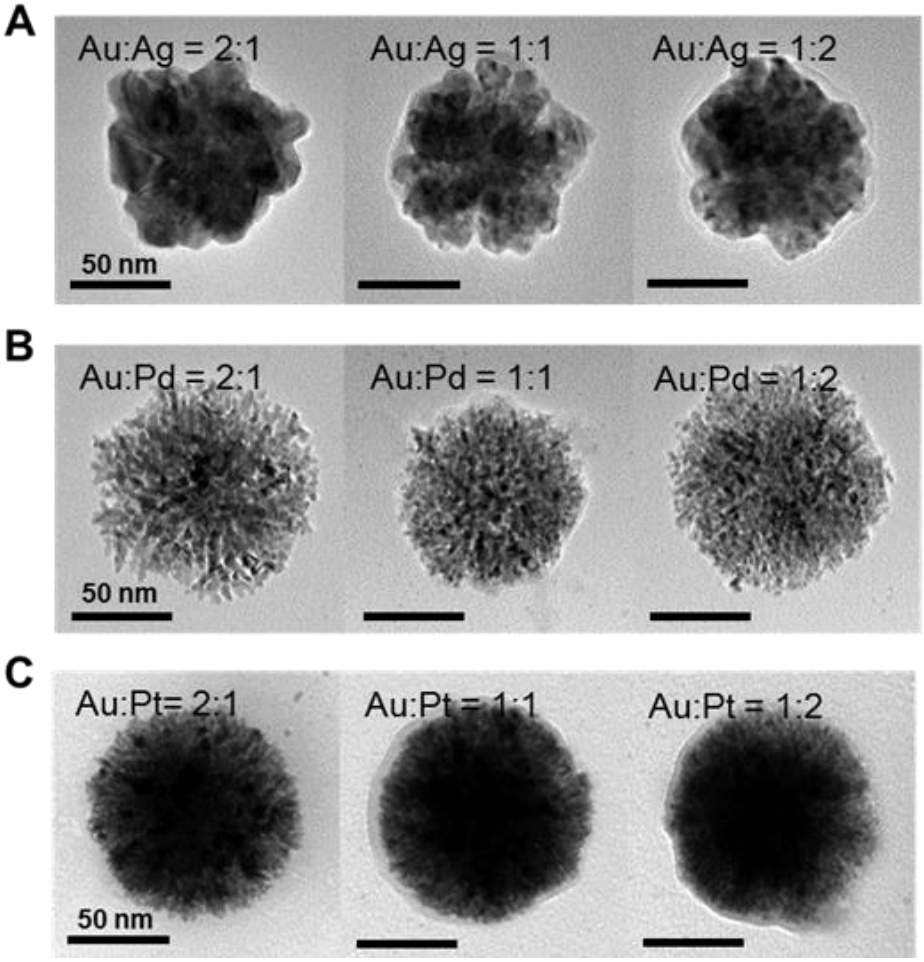

fig. S14. Representative TEM images of liposome/bimetallic hybrids synthesized from different precursor molar ratios. (A, **B**, and **C)** Representative TEM images of liposome/bimetallic hybrids synthesized from the precursor molar ratios of 2:1, 1:1, and 1:2, respectively (A: Au-Ag, B: Au-Pd, C: Au-Pt).

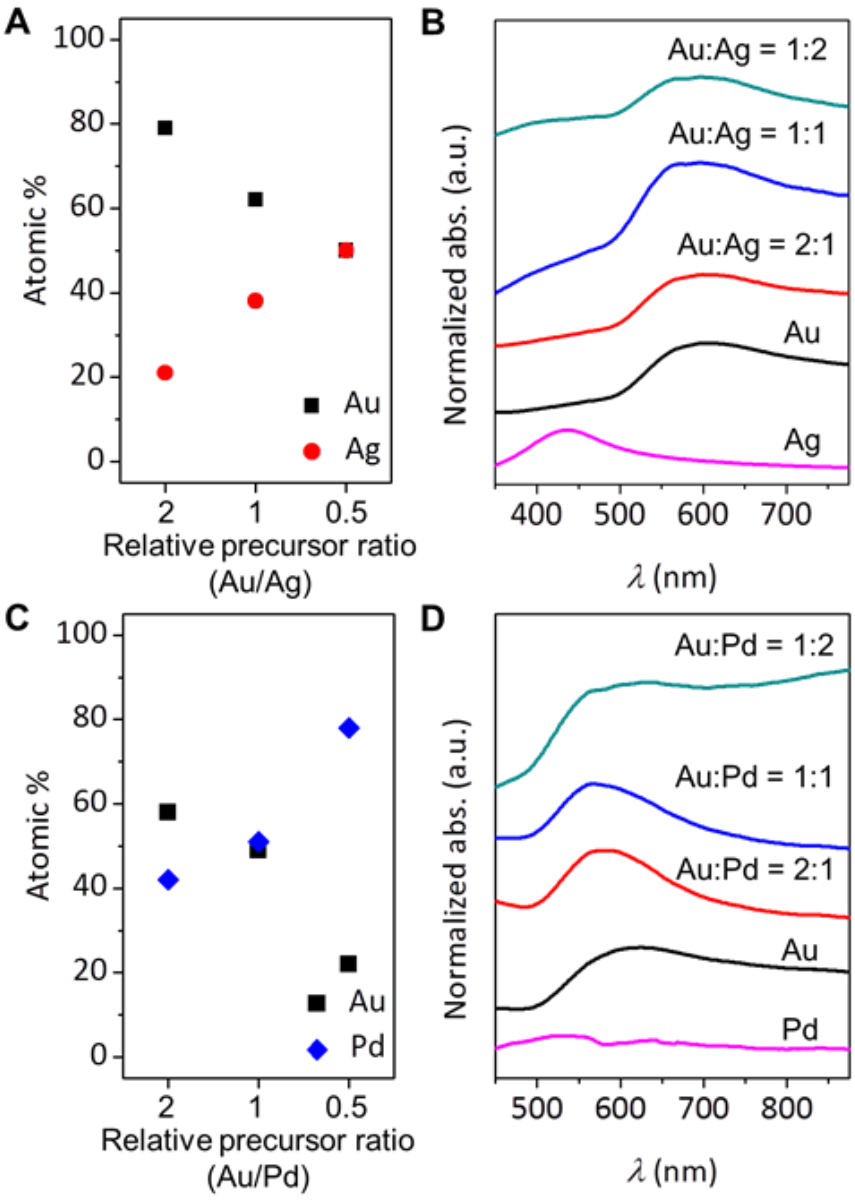

fig. S15. Atomic percentages and absorbance spectra of liposome/Au-Ag hybrids and liposome/Au-Pd hybrids synthesized from different precursor molar ratios. (A and **B)** Atomic percentages (A) and absorbance spectra (B) of liposome/Au-Ag hybrids synthesized from the precursor molar ratios of 2:1 (Au:Ag), 1:1, and 1:2, respectively. **(C** and **D)** Atomic percentages (C) and absorbance spectra (D) of liposome/Au-Pd hybrids synthesized from the precursor molar ratios of 2:1 (Au:Pd), 1:1, and 1:2, respectively.

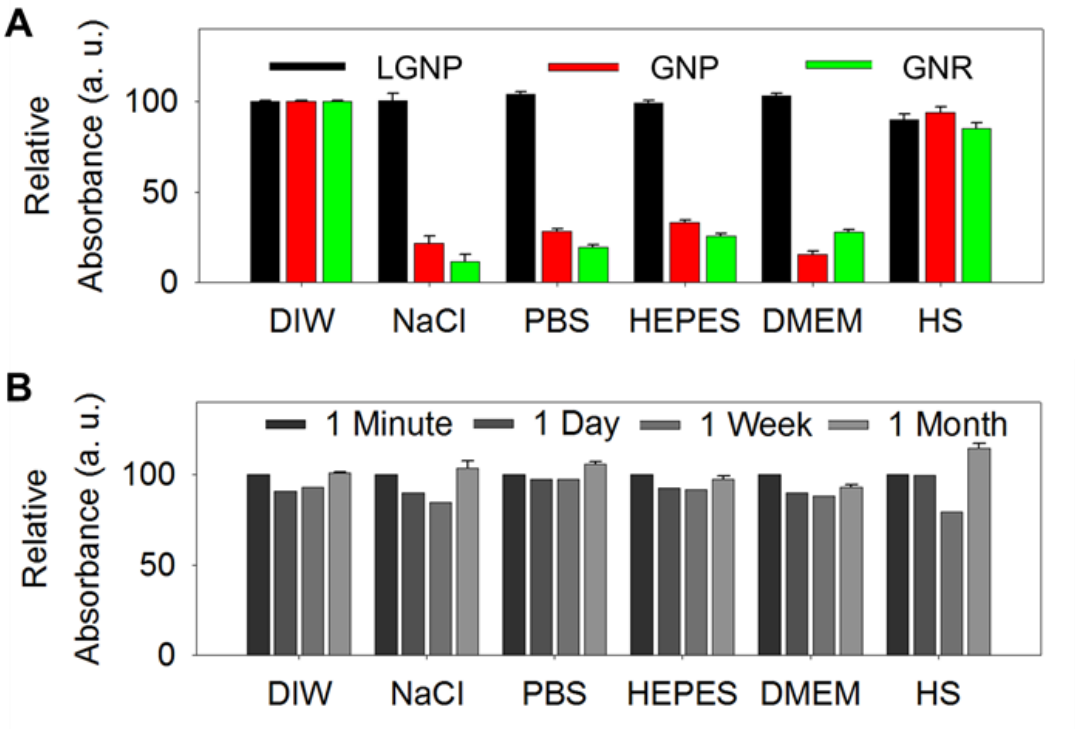

fig. S16. Representative relative absorbance at the SPR peaks of LGNP, GNP, and GNR under a wide variety of biologically relevant solutions and representative relative absorbance of LGNP with time duration of up to 1 month. (A) Representative relative absorbance at the SPR peaks of LGNP (541 nm), GNP (571 nm) and GNR (786 nm) under a wide variety of biologically relevant solutions. **(B)** Representative relative absorbance of LGNP with time duration up to 1 month. [DIW (deionized water), NaCl (sodium chloride), PBS (phosphate buffered saline pH 7.4), HEPES (4-(2-hydroxyethyl)-1-piperazineethanesulfonic acid), cell culture medium (Dulbecco's Modified Eagle's Medium (DMEM) high glucose), HS (human serum)].

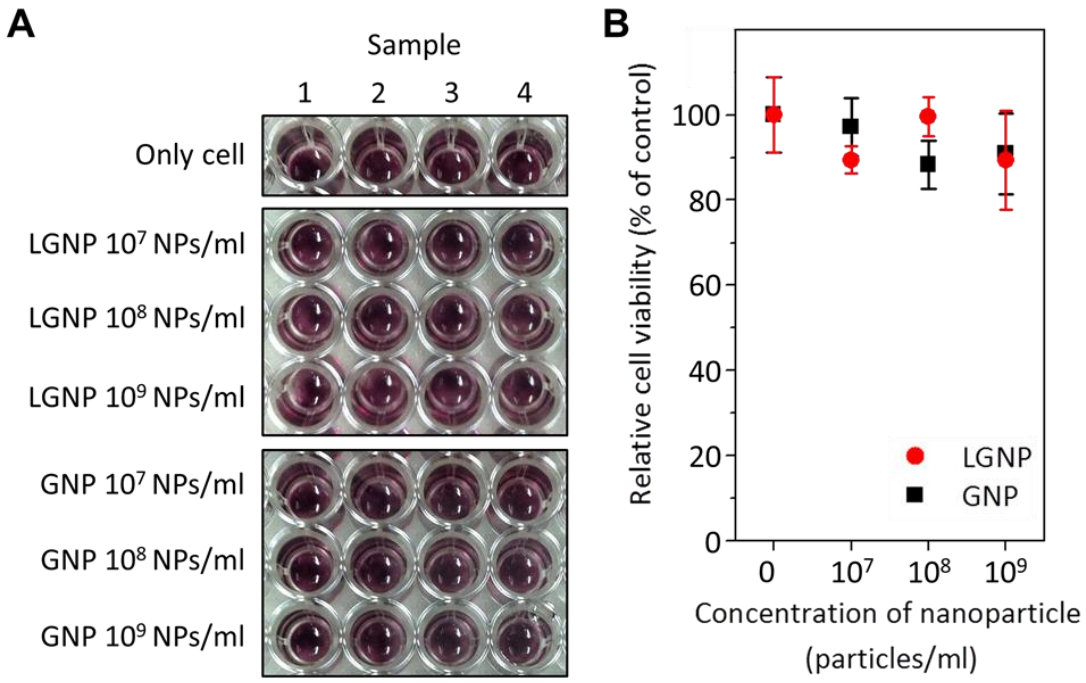

fig. S17. Viability of U-87 MG cells treated with LGNP and GNP solutions. (A) Representative photographs of MTT assay for the cells treated with LGNP and GNP solutions. **(B)** Relative cell viability based on the MTT assay.

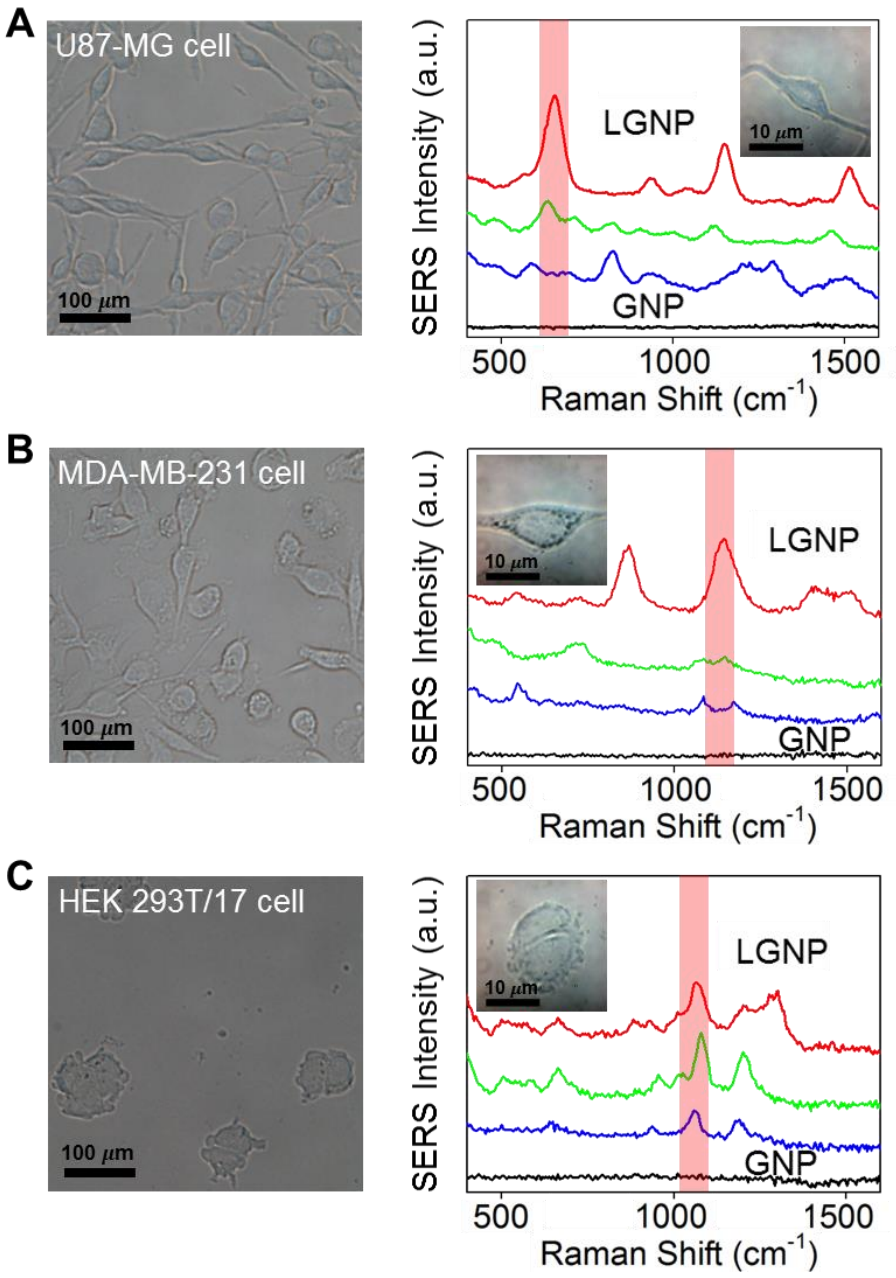

fig. S18. Optical microscope images and Raman spectra obtained from various cells after being treated with LGNP and GNP. (A, **B**, and **C)** Representative optical microscope images and surface-enhanced Raman spectra obtained from U-87MG cells (A), MDA-MB-231 cells (B), and HEK 293T/17 cells (C) after being treated with LGNP (red, green and blue lines) and GNP (black line) (inset in the spectra: optical microscope images of cells where the spectra were measured).

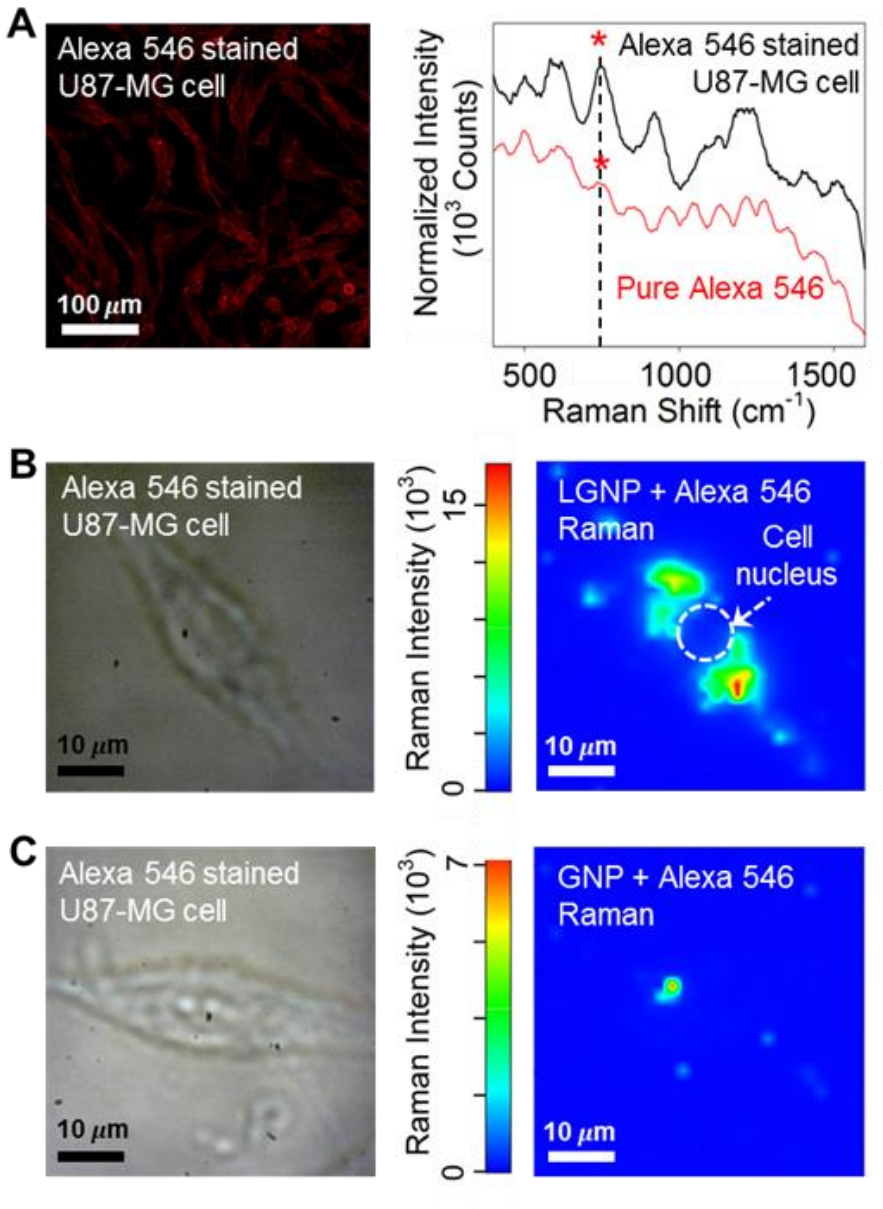

fig. S19. Fluorescent image and Raman spectra obtained from Alexa Fluor 546–stained U-87 MG cells, and optical microscope images and Raman maps obtained from Alexa Fluor 546–stained U-87MG cells after being treated with LGNP and GNP. (A) Fluorescent image and Raman spectra obtained from Alexa Fluor® 546 stained U-87MG cells (black line) and pure Alexa Fluor® 546 (red line). Characteristic Raman transition of Alexa Fluor® 546 that does not overlap with the Raman transitions of U-87MG cell is assigned by red asterisks (734 cm^{-1}). **(B** and **C)** Optical microscope images

and Raman maps obtained from Alexa Fluor® 546 dye stained U-87MG cells after being treated with LGNP (B) and GNP (C).

table S1. Calculated relative atomic percentages of gold and oxygen atoms in LGNP.

Au atom	
Volume of Au nanoparticle with 95 nm in diameter (nm^3)	*ca.* 5.23×10^5
Volume of unit cell for Au with face centered cubic lattice (nm^3)	*ca.* 6.79×10^{-2}
Number of Au atom in a unit cell	4
Total number of Au atom in Au nanoparticle with 95 nm in diameter	*ca.* 2.64×10^7
O atom	
Total number of lipid (DSPC) per liposome with 100 nm in diameter	*ca.* 7.47×10^4
Total number of O atom in lipid (DSPC) in liposome with 100 nm in diameter	*ca.* 5.97×10^5
Total number of reducing agent (ascorbic acid) per liposome with 100 nm in diameter	*ca.* 8.08×10^4
Total number of O atom in reducing agent (ascorbic acid) per liposome with 100 nm in diameter	*ca.* 4.85×10^5

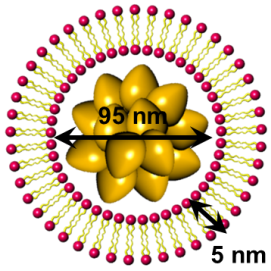

Liposome/Au hybrid	
Element	Atomic %
Au	96.1
O	3.9

table S2 The number of metal atoms per unit volume in liposome/Au, liposome/Ag, and liposome/Pd hybrids, measured by inductively coupled plasma atomic emission spectroscopy.

Particle	Metal concentration in sample (ppm)	Molecular weight of metal (g/mole)	Number of metal atom per unit volume
Liposome/Au hybrid	5.16 (Au)	196.97 (Au)	1.58×10^{19}
Liposome/Ag hybrid	2.43 (Ag)	107.87 (Ag)	1.36×10^{19}
Liposome/Pd hybrid	3.84 (Pd)	106.42 (Pd)	2.17×10^{19}